

Insight into phosphate adsorption on lanthanum hydroxide nanoparticle: influence of lanthanum/hydroxide molar ratio, performance, and mechanism study

Hongyuan Qin^a, Jiawei Huang^a, Xueli Zhang^a, Ling Yu^b, Yang Yu^{a,*}

^aGuangdong Key Laboratory of Environmental Pollution and Health, School of Environment, Jinan University, Guangzhou – 511443, China, emails: yuyang@jnu.edu.cn (Y. Yu), 944522368@qq.com (H. Qin), huangjiawei01@stu2017.jnu.edu.cn (J. Huang), 1137876059@qq.com (X. Zhang)

^bAnalysis and Test Center, Guangdong University of Technology, Guangzhou – 510006, China, email: yuling@gdut.edu.cn (L. Yu)

Received 3 September 2019; Accepted 10 February 2020

ABSTRACT

In this study, lanthanum hydroxide adsorbent was synthesized through a simple hydrothermal method and applied for removing phosphate from water. The optimal adsorbent was obtained at the La/OH molar ratio of 4:1. The adsorbent showed rapid adsorption of phosphate within the first 4 h in which approximately 84% of the equilibrium adsorption capacity can be achieved. The phosphate uptake was highly dependent on solution pH. The better fit of the Langmuir isotherm model to experimental data indicated that the monolayer adsorption occurred and the maximum adsorption capacity of 193.9 mg/g was accomplished at pH 7.0. The presence of fluoride could significantly retard the uptake of phosphate. X-ray photoelectron spectroscopy analysis indicated that hydroxyl groups on the adsorbent surface played the most key role in the adsorption. The phosphate ions were adsorbed on the adsorbent through the formation of inner-sphere complexes.

Keywords: Adsorption; Phosphate; Eutrophication; Lanthanum hydroxide nanoparticle; Hydrothermal synthesis

1. Introduction

Phosphate as an essential nutrient for the growth of aquatic organisms has been classified as one of the important factors causing the eutrophication of lakes, lagoons, rivers, and coastal seas [1]. To prevent eutrophication problem, the maximum concentration of phosphorus in the water is recommended as lower than 50 µg/L by the United States Environmental Protection Agency. Since the excessive discharge of phosphate from industrial wastewater and agricultural/household activities is considered as the main reason for the limit-exceeding problem of phosphate in waters, the World Health Organization has also set a maximum discharge limit of phosphorus of 0.5–1 mg/L.

Therefore, the development of effective techniques for phosphate removal from wastewater is urgently needed.

Various technologies including chemical precipitation, ion exchange, membrane filtration, biological treatment, and adsorption have been extensively studied and applied for the removal of phosphate from water. Among them, adsorption is considered as one of the most attracting methods due to its advantages of high selectivity, low cost, and flexibility in operation [2,3]. Numerous adsorbents have been developed for the phosphate removal from water, including red mud [4], fly ash [5], layered double hydroxides [6], iron oxides [7], metal oxide-based adsorbents [8], and carbon-based materials [9,10]. Especially, the excellent adsorption performance of lanthanum-based adsorbents

* Corresponding author.

has attracted increasing attention in the last decade as a result of the higher affinity of lanthanum toward phosphate than other conventional metals [11,12]. In our previous study, a Fe–Mg–La trimetal composite adsorbent was synthesized by a simple co-precipitation method, which had a maximum adsorption capacity of 451.2 mg/g at pH 6.0 [13]. The abundant content of hydroxyl groups on the adsorbent surface was verified to be responsible for its extremely high uptake of phosphate. Accordingly, the metal hydroxide generally exhibits a better adsorption performance than the corresponding metal oxide [14]. The hydrothermal synthetic route can obtain more uniform metal hydroxide/oxide adsorbents with smaller particle size [15]. Moreover, the physico-chemical properties of adsorbent can be adjusted by controlling conditions of the hydrothermal synthesis procedure, for example, concentrations of NaOH and precursor salts [16].

In the present work, we prepared lanthanum hydroxide nanoparticles through a simple hydrothermal method. The influence of lanthanum/hydroxide (La/OH) molar ratio in properties and adsorption performance was investigated. A series of batch experiments were conducted to study the adsorption kinetics and isotherm, and influences of solution pH, co-existing anions, and ionic strength on the uptake of phosphate. X-ray photoelectron spectroscopy (XPS) was employed for better understanding the possible adsorption mechanism.

2. Materials and methods

2.1. Materials

All chemicals used in this study, including $\text{La}(\text{NO}_3)_3 \cdot 6\text{H}_2\text{O}$, NaOH, HNO_3 , KH_2PO_4 , NaCl, NaF, Na_2CO_3 , and Na_2SO_4 , were of reagent grade without further purification and purchased from Aladdin Chemicals (Shanghai, China). Phosphate stock solution of 1,000 mg/L was prepared by dissolving KH_2PO_4 in deionized (DI) water. Each test solution was freshly prepared by diluting phosphate stock solution with DI water.

2.2. Adsorbent preparation

Lanthanum hydroxide adsorbents with different La/OH molar ratios were synthesized through a simple hydrothermal method. In brief, 4.33 g of $\text{La}(\text{NO}_3)_3 \cdot 6\text{H}_2\text{O}$ was dissolved into 100 mL DI water and stirred for 30 min. Then, a predetermined amount of 0.1 M NaOH was dropwise added into the solution under continuous agitation. The suspension was transferred into a 100 mL Teflon-line autoclave at 150°C for 8 h. The obtained precipitate was collected by a centrifuge, washed by DI water for at least three times and dried in oven at 60°C overnight. The dried particles were ground into fine powders using an agate mortar for the experiments.

2.3. Characterization

Surface morphology of lanthanum hydroxide nanoparticles was observed by scanning electron microscope (SEM, ZEISS EVO18, Germany). The crystalline phases

of adsorbents were visualized by X-ray diffraction (XRD, Bruker D2 Phaser, Germany) using copper $\text{K}\alpha$ radiation with 2θ scan range of 10°–80° and a step size of 0.02°. The surface element distribution and composition of carbon or oxygen containing groups were analyzed by XPS (Kratos XPS system-Axis His-165 Ultra, Shimadzu, Japan) at 15 KV, 10 mA, and a base pressure of 3×10^{-8} Torr in the chamber with an Al $\text{K}\alpha$ X-ray source (150 W). All XPS results in binding energy forms were fitted using a nonlinear least squares curve fitting program (XPSPEAK Software, Version 4.1).

2.4. Adsorption experiments

The adsorption kinetics experiment was conducted at an initial phosphate concentration of 20 mg/L. The solution pH was adjusted to 7.0 and maintained throughout the experiment by adding HNO_3 or NaOH. Samples were taken under different time intervals and filtered using 0.45 μm cellulose syringe membranes. The concentration of phosphate was determined using an inductively coupled plasma mass spectrometry.

In the experiment of pH effect, the initial phosphate concentration was 20 mg/L, and the adsorbent dosage was 0.1 g/L. The solution pH was controlled throughout the experiment in varied values ranging from 3.0 to 10.0. After agitation for 24 h, samples were taken for the analysis of the phosphate concentration. In order to investigate the role of hydroxyl groups from the adsorbent in the adsorption of phosphate, pH of phosphate solutions was initially adjusted at 3.0–10.0 without further control throughout the adsorption process. Other experimental conditions were the same as aforementioned procedure. After stirred for 24 h, final solution pH was measured.

In the experiment of adsorption isotherm, 0.01 g of adsorbents were, respectively, added into phosphate solutions with concentrations ranging from 5 to 80 mg/L. The solution pH was adjusted to 7.0. Other experimental steps were same as those of pH effect experiment.

In the experiment of adsorption selectivity, a certain amount of NaF, NaCl, Na_2SO_4 and Na_2CO_3 were added into phosphate solutions with the initial phosphate concentration of 20 mg/L, respectively. The solution pH was maintained at 7.0 during the adsorption. Other experimental steps were same as the pH effect experiment.

In the experiment of ionic strength effect, different amounts of sodium nitrate were added into 20 mg/L phosphate solutions to elevate the background ionic strength to 1, 10, and 100 mM, respectively. The solution pH was adjusted to 7.0. Other experimental steps were same as the pH effect experiment.

3. Results and discussion

3.1. Influence of La/OH molar ratio

Different La/OH molar ratios were used to prepare lanthanum hydroxide adsorbents and the adsorption capacities of adsorbents toward phosphate are shown in Fig. 1. The adsorption capacity of adsorbent is significantly affected by the La/OH molar ratio. The optimal adsorption

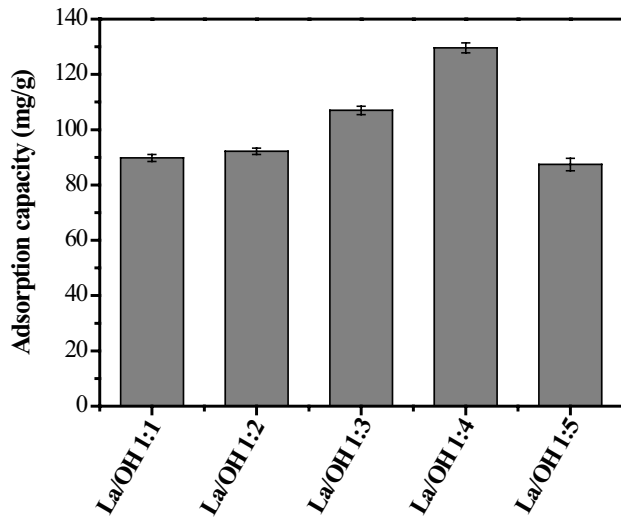


Fig. 1. Influence of La/OH molar ratio on phosphate uptake. Initial phosphate concentration = 20 mg/L; adsorbent dosage = 0.1 g/L; pH = 7.0; $T = 25^{\circ}\text{C} \pm 1^{\circ}\text{C}$.

performance of 129.6 mg/g at pH 7.0 is achieved by the adsorbent with the La/OH molar ratio of 1:4. With the further increase in the La/OH molar ratio, the adsorption is found to be reduced.

As shown in Fig. S1, with the increase in the La/OH molar ratio, the adsorbent seems to have a more compact structure. As illustrated in Fig. S2, the characteristic peaks at 20.4° , 23.7° , 29.8° , 38.0° , 43.3° , 44.6° , and 45.9° , which can be detected in the XRD pattern of La/OH 1:1 adsorbent, are assigned to lanthanum carbonate hydroxide (PDF No. 49-0981). As reported in our previous study, carbonate groups might be introduced into the adsorbent when the adsorbent was prepared under open-air condition [17]. With the increase in the La/OH molar ratio, the aforementioned peaks become gradually weak and disappeared, suggesting that the formation of lanthanum carbonate hydroxide is restrained. The typical crystal structure of lanthanum hydroxide particles (PDF No. 36-1481) can be observed in the XRD pattern of the La/OH 1:4 adsorbent. The crystallization behavior of the lanthanum hydroxide is found to be slightly disturbed by the further increase in the La/OH molar ratio. Therefore, the crystal structure of lanthanum hydroxide adsorbents might play a certain role in adsorption performance and the adsorbent with the La/OH molar ratio of 1:4 was chosen to further investigate the adsorption behavior and mechanism.

3.2. Adsorption kinetics

As shown in Fig. 2a, the adsorption equilibrium with an adsorption capacity of 139.2 mg/g at pH 7.0 can be reached within 10 h. The adsorption rate of phosphate is relatively rapid within the first 4 h in which approximately 84% of the equilibrium removal can be achieved.

The experimental data was further fitted by the pseudo-first-order and pseudo-second-order models. The corresponding parameters are illustrated in Table 1. According to the correlation coefficient (r^2), the experimental data can be

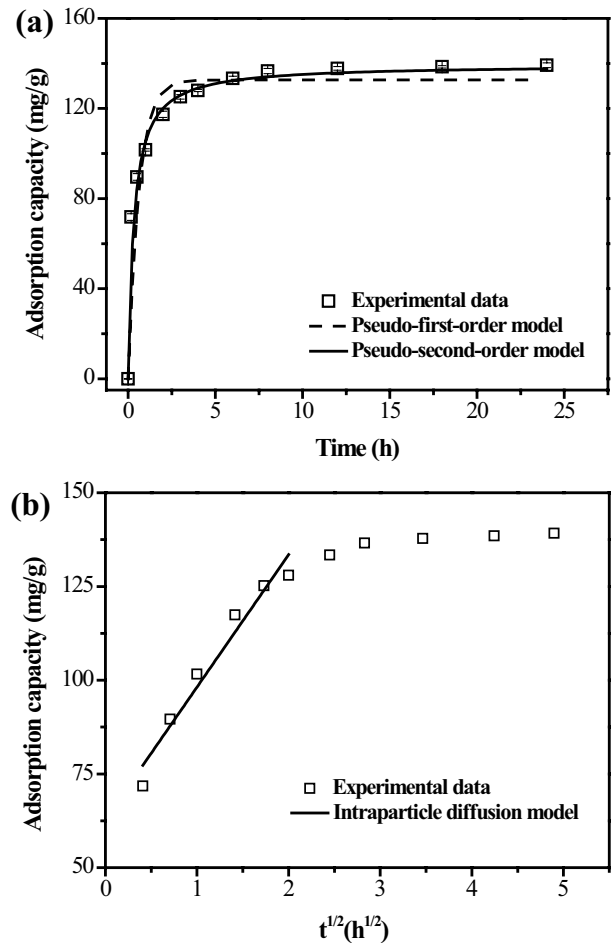


Fig. 2. Adsorption kinetics of phosphate at pH 7.0 (a) experimental data and fitting results of the pseudo-first-order and pseudo-second-order models and (b) the intraparticle diffusion model. Initial phosphate concentration = 20 mg/L; adsorbent dosage = 0.1 g/L; $T = 25^{\circ}\text{C} \pm 1^{\circ}\text{C}$.

better fitted by the pseudo-second-order model than pseudo-first-order model, suggesting that the uptake of phosphate is mainly governed by a chemisorption process.

The rate-limiting step of the adsorption process was explored using the intraparticle diffusion model. The mathematical equation of the model is expressed as follows:

$$q_t = K_{id}t^{1/2} + \alpha \quad (1)$$

where q_t (mg/g) is the adsorption capacity of phosphate on the adsorbent at time t (h), K_{id} ((mg/g)/h^{1/2}) is the rate constant of the intraparticle diffusion model, and α (mg/g) refers to the boundary layer effect.

As shown in Fig. 2b, the plot of q_t against $t^{1/2}$ shows a straight line at the initial stage of adsorption process, indicating that the intraparticle diffusion is involved in the adsorption of phosphate on the adsorbent. According to the value of α illustrated in Table 1, approximately 46.5% of ultimate adsorption capacity is affected by the effect of boundary layer. Noted that this portion of adsorption

Table 1
Constants of adsorption kinetics models

Pseudo-first-order			Pseudo-second-order			Intraparticle diffusion		
K_1 (h^{-1})	q_e (mg/g)	r^2	K_2 (g/mg/h)	q_e (mg/g)	r^2	K_{id} ((mg/g)/h ^{1/2})	α (mg/g)	r^2
2.961	128.5	0.91	0.034	135.9	0.98	35.31	62.86	0.95

capacity can be rapidly accomplished within 10 min. After the linear stage, there is around 8% of ultimate adsorption capacity occurred during the followed 20 h. The adsorption rate significantly slows down due to the low phosphate concentration in solution [18]. Thus, the adsorption rate of phosphate tends to be mainly limited by the intraparticle diffusion process.

3.3. pH effect

As shown in Fig. 3, the higher adsorption of phosphate takes place under acidic and neutral conditions, and there is no obvious difference in adsorption capacities when solution pH is in the range of 3.0–7.0. With a further increase in solution pH, the uptake of phosphate remarkably decreases. At pH above 7.0, more OH⁻ ions are present in the solution which may strongly depress the exchange process between hydroxyl groups on the adsorbent surface and phosphate ions [13]. Solution pH change after the adsorption process was shown in Fig. S3. It can be seen that solution pH is elevated over the whole pH range. Since pH of phosphate solutions was only initially adjusted at predetermined values, the increasing concentration of hydroxide ions in solutions is likely due to the release of hydroxyl groups from the adsorbent during the adsorption.

3.4. Adsorption isotherm

In order to better understand the adsorption process, the Langmuir and Freundlich isotherm models were used to exploit fundamental physico-chemical information. The corresponding equations are expressed as follows:

$$q_e = \frac{q_{\max} b C_e}{1 + b C_e} \quad (2)$$

$$q_e = K_f C_e^{1/n} \quad (3)$$

where q_e and C_e are the amount of phosphate adsorbed on the adsorbent (mg/g) and the equilibrium concentration of phosphate in solution (mg/L), respectively. q_{\max} is the theoretical maximum adsorption capacity of the adsorbent (mg/g), and b is the equilibrium adsorption constant related to the affinity of binding sites (L/mg). K_f ($\text{mg}^{(1-1/n)} \text{L}^{1/n}/\text{g}$) is a constant for relative adsorption capacity, and n is the heterogeneity factor which has a lower value for more heterogeneous surfaces.

The experimental data of adsorption isotherm at pH 7.0 and the fit of both the Langmuir and Freundlich isotherm models are shown in Fig. 4. The model constants are summarized in Table 2. Based on the correlation coefficient

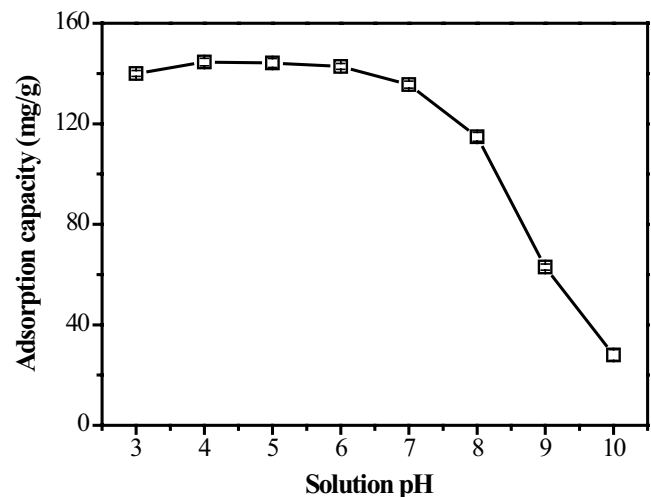


Fig. 3. Influence of solution pH on phosphate uptake. Initial phosphate concentration = 20 mg/L; adsorbent dosage = 0.1 g/L; $T = 25^\circ\text{C} \pm 1^\circ\text{C}$.

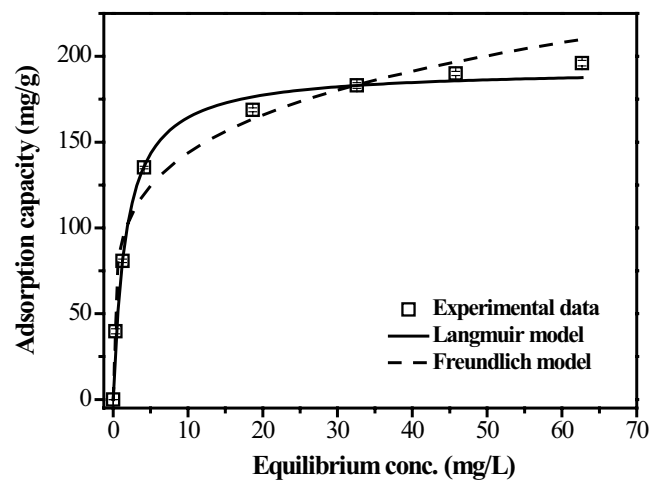


Fig. 4. Adsorption isotherm of phosphate on the adsorbent at pH 7.0. Adsorbent dosage = 0.1 g/L; $T = 25^\circ\text{C} \pm 1^\circ\text{C}$.

Table 2
Langmuir and Freundlich isotherm parameters for phosphate adsorption

Langmuir isotherm			Freundlich isotherm		
q_{\max} (mg/g)	b (L/mg)	r^2	K_f ($\text{mg}^{(1-1/n)} \text{L}^{1/n}/\text{g}$)	$1/n$	r^2
193.9	0.586	0.99	81.36	0.227	0.95

(r^2), the experimental data is found to be better simulated by the Langmuir model than the Freundlich model. This indicates that the phosphate uptake is mainly controlled by the monolayer adsorption process. The maximum adsorption capacity of adsorbent toward phosphate is 193.9 mg/g, much higher than most of previously reported adsorbents [9,19–21].

The adsorption favorability of phosphate on the adsorbent can be evaluated according to the value of the Freundlich constant, $1/n$, which is related to the adsorption intensity. Generally, the adsorption is considered to be favorable when $0.5 < 1/n \leq 1$, more favorable when $0.1 < 1/n \leq 0.5$, and unfavorable as $1/n > 1$ [22]. As listed in Table 2, the value of $1/n$ is calculated as 0.227, suggesting that the phosphate could be favorably adsorbed on the adsorbent surface.

3.5. Influence of competitive anions and ionic strength

Such anions as carbonate, sulfate, fluoride, and chloride commonly exist in water and could compete with phosphate for the adsorptive sites on the adsorbent. Therefore, it is of crucial importance to evaluate the effect of their presence on the phosphate uptake. As shown in Fig. 5, more obvious interference in the adsorption is caused by increasing concentrations of these competitive anions. The presence of fluoride in solution has the most significantly negative effect on the uptake of phosphate, which may be due to the strong competition of fluoride with phosphate. The high affinity of lanthanum-based adsorbents toward fluoride has been extensively reported in the literature [23,24].

Since surface properties of adsorbent may be affected by the background ionic strength, the effect of ionic strength on the phosphate adsorption was investigated. In addition, the dependency of the adsorption capacity on ionic strength can be used for identifying the type of surface complexes (e.g., the inner- and outer-sphere). When the phosphate is weakly bonded on the adsorbent surface, the outer-sphere surface complexes are considered to be formed and the uptake of phosphate would be significantly depressed by increasing the ionic strength. In contrast, the strongly bonded phosphate ions are generally in the form of inner-sphere surface complexes in which the adsorption would be insensitive to the background ionic strength. As shown in Fig. 6, the ionic strength shows a negligible influence in the adsorption capacity of adsorbent, suggesting that the inner-sphere surface complexes should be formed during the adsorption.

3.6. Mechanism study

As shown in Fig. 7, the characteristic peaks of La, O, and C elements, including La 4d, La 4p, La 3d, C 1s, O 1s, and O KL1, can be detected in the wide-scan XPS spectrum of virgin adsorbent. After the adsorption, a new peak assigned to P 2p appears in the spectrum of the P-loaded adsorbent. The high-resolution XPS spectrum of P element is given in Fig. S4.

Based on the results from XRD analysis, carbonate groups may be present on the adsorbent surface and participate in the adsorption process. The high-resolution C 1s XPS spectra of adsorbents before and after the adsorption were investigated. As shown in Fig. 8, the main peak

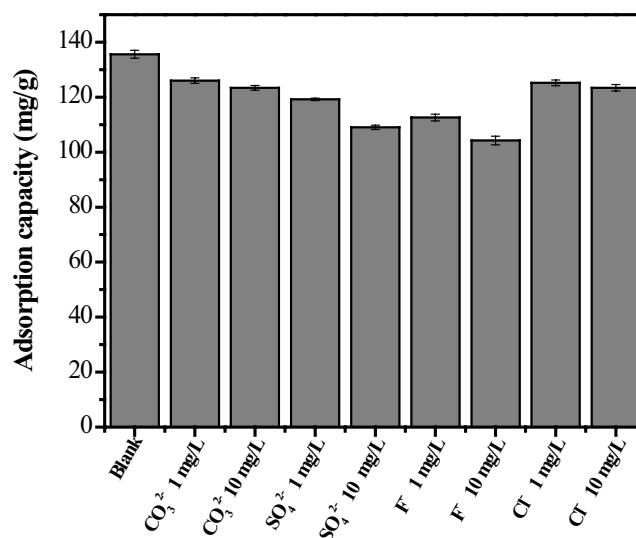


Fig. 5. Effect of co-existing anions on phosphate uptake. Initial phosphate concentration = 20 mg/L; adsorbent dosage = 0.1 g/L; $T = 25^\circ\text{C} \pm 1^\circ\text{C}$; $\text{pH} = 7.0$.

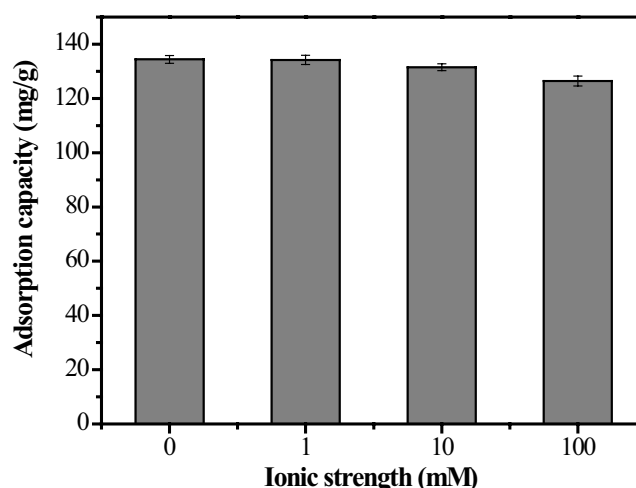


Fig. 6. Effect of ionic strength on phosphate uptake. Initial phosphate concentration = 20 mg/L; adsorbent dosage = 0.1 g/L; $T = 25^\circ\text{C} \pm 1^\circ\text{C}$; $\text{pH} = 7.0$.

at the binding energy of 284.9 eV is attributed to reference C 1s, which is caused by exposure to ambient atmosphere. The peak at the binding energy of 289.3 eV is attributed to the presence of carbonate groups on the adsorbent surface [17]. After the adsorption, the relative content of carbonate groups decreases from 45.1% to 23.6%, indicating that carbonate groups may participate in the adsorption process. It is worthwhile to note that the strength of C 1s peaks in the wide-scan XPS spectra of virgin and P-loaded adsorbents is quite weak. The role of carbonate groups in the uptake of phosphate could be therefore considered neglectful compared to hydroxyl groups. This is consistent with results of the experiment of La/OH molar ratio effect and XRD analysis.

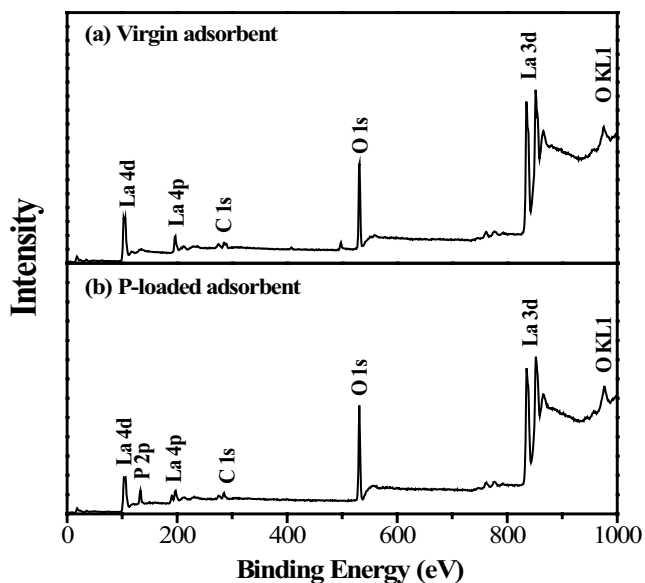


Fig. 7. XPS wide-scan spectra of the adsorbents before and after the phosphate adsorption. (a) Virgin adsorbent and (b) P-loaded adsorbent.

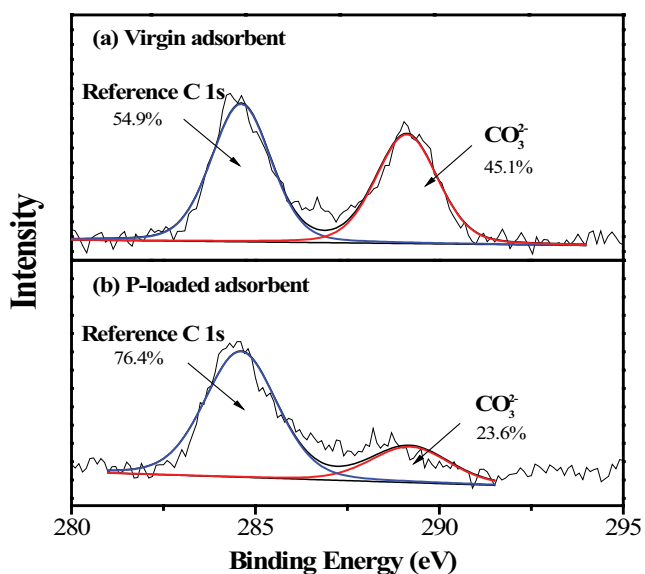


Fig. 8. High-resolution C 1s XPS spectra of the adsorbents before and after the adsorption. (a) Virgin adsorbent and (b) P-loaded adsorbent.

The high-resolution O 1s XPS spectra of adsorbents before and after the adsorption were investigated to evaluate the role of hydroxyl groups in the adsorption. As shown in Fig. 9, the O 1s spectra can be divided into three component peaks at the binding energies of 530.2, 531.0, and 532.7 eV, which are assigned to metal–oxygen bond (M–O), hydroxyl group bonded metal atom (M–OH), and adsorbed water (H₂O), respectively. After the adsorption, the content of M–OH decreases from 75.6% to 65.8%, while the contents of M–O and adsorbed H₂O increase from 9.5% to 23.2% and 10.9% to 11.0%, respectively. The remarkable reduction

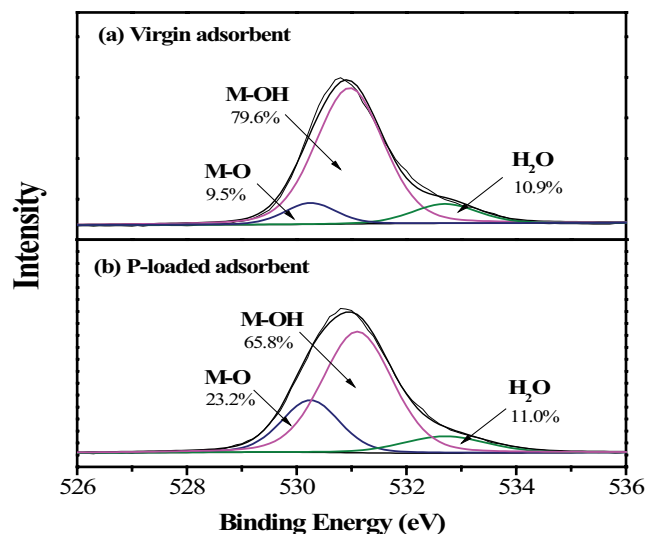


Fig. 9. High-resolution O 1s XPS spectra of the adsorbents before and after the adsorption. (a) Virgin adsorbent and (b) P-loaded adsorbent.

in the content of M–OH clearly indicates that hydroxyl groups bonded on metal atoms would be highly involved in the adsorption process.

From the results of batch experiments and spectroscopy analysis, the ligand exchange between phosphate ions and hydroxyl groups or carbonate groups on the adsorbent is proposed as the adsorption mechanism. The hydroxyl groups should play a more important role in the uptake of phosphate than carbonate groups. The phosphate ions are adsorbed on the adsorbent through the formation of inner-sphere surface complexes.

4. Conclusions

Lanthanum hydroxide nanoparticles were synthesized through a simple hydrothermal method and applied for the effective removal of phosphate. The crystal structure of adsorbent can be highly affected by the La/OH molar ratio, and the adsorbent with the La/OH molar ratio of 1:4 performed better on the adsorption of phosphate. The optimal uptake can be obtained in the pH range of 3.0–7.0. The kinetics study showed that approximately 84% of the equilibrium adsorption capacity can be achieved within the initial 4 h and the adsorption equilibrium reached within 10 h. The maximum adsorption capacity at pH 7.0 was 193.9 mg/g, much higher than most of previously reported adsorbents. The most significant interference in the adsorption was caused by the presence of fluoride. During the adsorption, the phosphate ions were exchanged with hydroxyl groups and adsorbed on the adsorbent surface in the form of inner-sphere complexes.

Acknowledgment

This research was supported by Natural Science Foundation of Guangdong Province (Grant No. 2018A0303130148).

References

- [1] T.H. Bui, S.P. Hong, J. Yoon, Development of nanoscale zirconium molybdate embedded anion exchange resin for selective removal of phosphate, *Water Res.*, 134 (2018) 22–31.
- [2] R. Li, J.J. Wang, B. Zhou, M.K. Awasthi, A. Ali, Z. Zhang, A.H. Lahori, A. Mahar, Recovery of phosphate from aqueous solution by magnesium oxide decorated magnetic biochar and its potential as phosphate-based fertilizer substitute, *Bioresour. Technol.*, 215 (2016) 209–214.
- [3] D. Jiang, Y. Amano, M. Machida, Removal and recovery of phosphate from water by calcium-silicate composites-novel adsorbents made from waste glass and shells, *Environ. Sci. Pollut. Res. Int.*, 24 (2017) 8210–8218.
- [4] Q. Yue, Y. Zhao, Q. Li, W. Li, B. Gao, S. Han, Y. Qi, H. Yu, Research on the characteristics of red mud granular adsorbents (RMGA) for phosphate removal, *J. Hazard. Mater.*, 176 (2010) 741–748.
- [5] S.G. Lu, S.Q. Bai, L. Zhu, H.D. Shan, Removal mechanism of phosphate from aqueous solution by fly ash, *J. Hazard. Mater.*, 161 (2009) 95–101.
- [6] R. Li, J.J. Wang, B. Zhou, M.K. Awasthi, A. Ali, Z. Zhang, L.A. Gaston, A.H. Lahori, A. Mahar, Enhancing phosphate adsorption by Mg/Al layered double hydroxide functionalized biochar with different Mg/Al ratios, *Sci. Total Environ.*, 559 (2016) 121–129.
- [7] Z. Hongshao, R. Stanforth, Competitive adsorption of phosphate and arsenate on goethite, *Environ. Sci. Technol.*, 35 (2001) 4753–4757.
- [8] R. Li, J.J. Wang, Z. Zhang, M.K. Awasthi, D. Du, P. Dang, Q. Huang, Y. Zhang, L. Wang, Recovery of phosphate and dissolved organic matter from aqueous solution using a novel CaO-MgO hybrid carbon composite and its feasibility in phosphorus recycling, *Sci. Total Environ.*, 642 (2018) 526–536.
- [9] Q. Yin, H. Ren, R. Wang, Z. Zhao, Evaluation of nitrate and phosphate adsorption on Al-modified biochar: influence of Al content, *Sci. Total Environ.*, 631–632 (2018) 895–903.
- [10] S. Vasudevan, J. Lakshmi, The adsorption of phosphate by graphene from aqueous solution, *RSC Adv.*, 2 (2012) 5234–5242.
- [11] H. Li, J. Ru, W. Yin, X. Liu, J. Wang, W. Zhang, Removal of phosphate from polluted water by lanthanum doped vesuvianite, *J. Hazard. Mater.*, 168 (2009) 326–330.
- [12] Y. He, L. Hai, Y. Dong, W. Liang, Preferable adsorption of phosphate using lanthanum-incorporated porous zeolite: characteristics and mechanism, *Appl. Surf. Sci.*, 426 (2017) 995–1004.
- [13] Y. Yang, J.P. Chen, Key factors for optimum performance in phosphate removal from contaminated water by a Fe–Mg–La tri-metal composite sorbent, *J. Colloid Interface Sci.*, 445 (2015) 303–311.
- [14] R. Chitrakar, S. Tezuka, A. Sonoda, K. Sakane, K. Ooi, T. Hirotsu, Selective adsorption of phosphate from seawater and wastewater by amorphous zirconium hydroxide, *J. Colloid Interface Sci.*, 297 (2006) 426–433.
- [15] Y. Yu, L. Yu, M. Sun, J. Paul Chen, Facile synthesis of highly active hydrated yttrium oxide towards arsenate adsorption, *J. Colloid Interface Sci.*, 474 (2016) 216–222.
- [16] T. Sakthivel, S. Das, A. Kumar, D.L. Reid, A. Gupta, D.C. Sayle, S. Seal, Morphological phase diagram of biocatalytically active ceria nanostructures as a function of processing variables and their properties, *ChemPlusChem*, 78 (2013) 1446–1455.
- [17] Y. Yu, L. Yu, J.P. Chen, Introduction of an yttrium-manganese binary composite that has extremely high adsorption capacity for arsenate uptake in different water conditions, *Ind. Eng. Chem. Res.*, 54 (2015) 3000–3008.
- [18] A.E. Ofomaja, Intraparticle diffusion process for lead(II) biosorption onto mansonia wood sawdust, *Bioresour. Technol.*, 101 (2010) 5868–5876.
- [19] J. Xie, Z. Wang, S. Lu, D. Wu, Z. Zhang, H. Kong, Removal and recovery of phosphate from water by lanthanum hydroxide materials, *Chem. Eng. J.*, 254 (2014) 163–170.
- [20] J. Lü, H. Liu, R. Liu, X. Zhao, L. Sun, J. Qu, Adsorptive removal of phosphate by a nanostructured Fe–Al–Mn trimetal oxide adsorbent, *Powder Technol.*, 233 (2013) 146–154.
- [21] H. Liu, X. Sun, C. Yin, C. Hu, Removal of phosphate by mesoporous ZrO₂, *J. Hazard. Mater.*, 151 (2008) 616–622.
- [22] R.E. Treybal, *Mass Transfer Operations*, McGraw-Hill, New York, 1980.
- [23] Y. Yu, C. Wang, X. Guo, J. Paul Chen, Modification of carbon derived from *Sargassum* sp. by lanthanum for enhanced adsorption of fluoride, *J. Colloid Interface Sci.*, 441 (2015) 113–120.
- [24] J. Wang, N. Chen, C. Feng, M. Li, Performance and mechanism of fluoride adsorption from groundwater by lanthanum-modified pomelo peel biochar, *Environ. Sci. Pollut. Res. Int.*, 25 (2018) 15326–15335.

Supplementary information

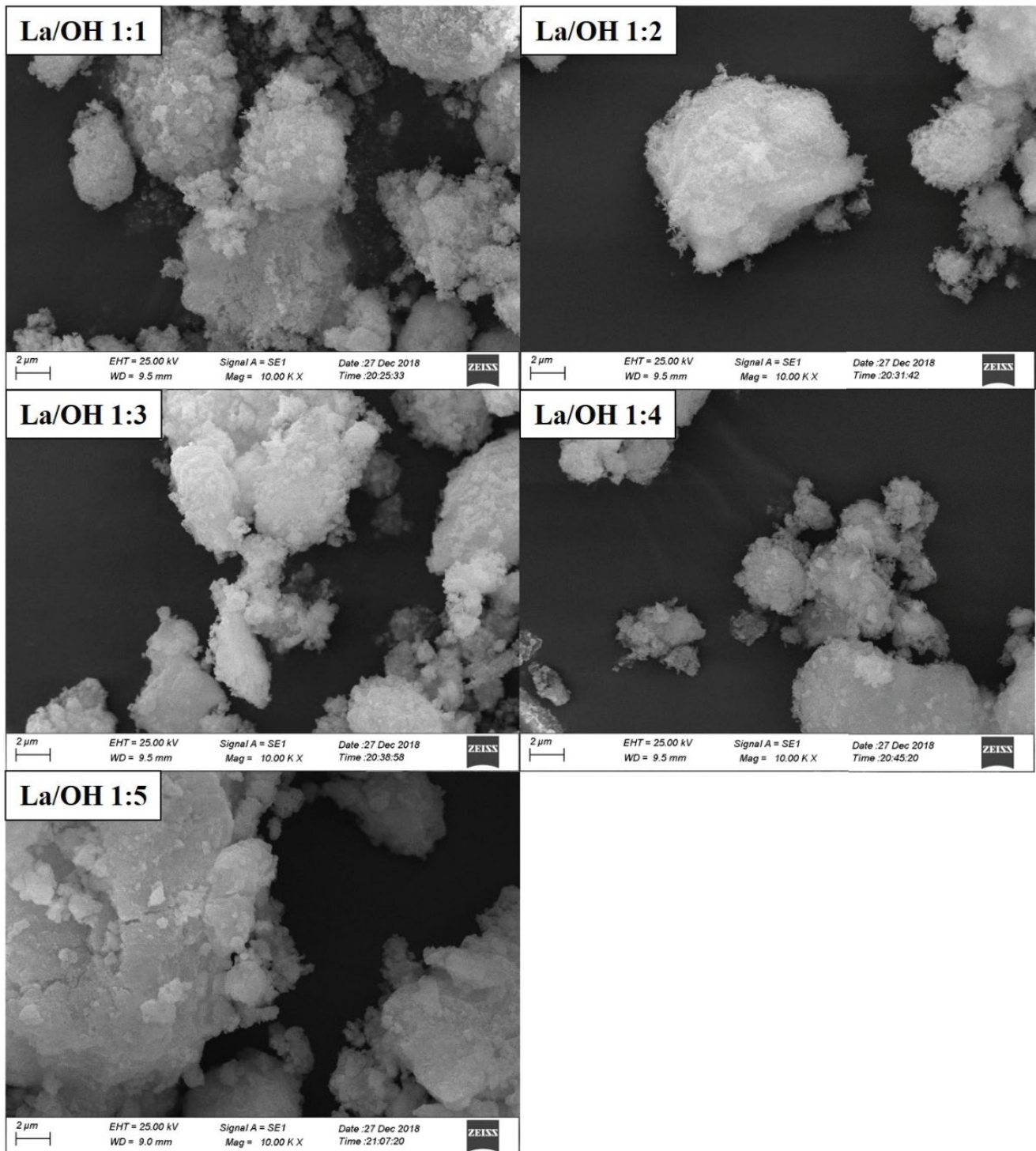


Fig. S1. SEM images of lanthanum hydroxide nanoparticles with different La/OH molar ratios.

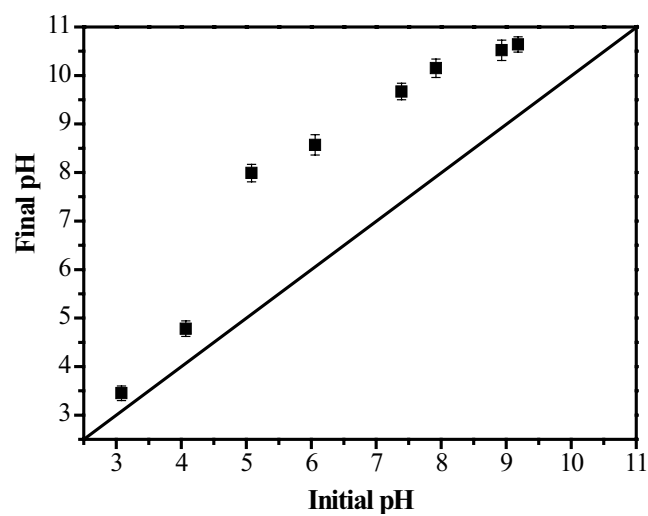
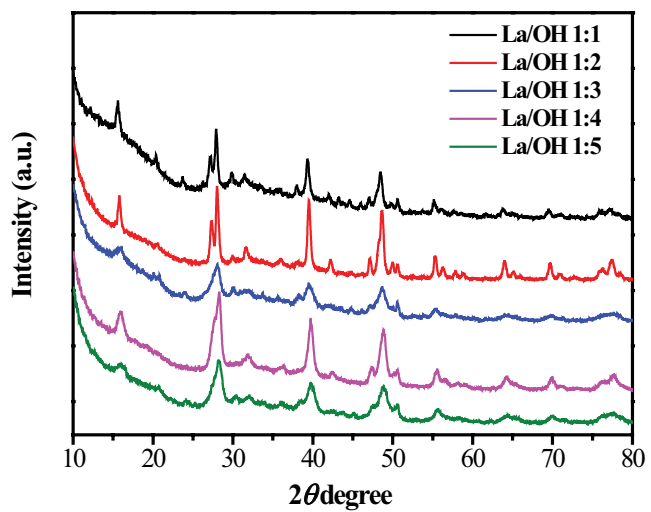


Fig. S2. XRD patterns of lanthanum hydroxide nanoparticles with different La/OH molar ratios.

Fig. S3. Solution pH change after the adsorption.

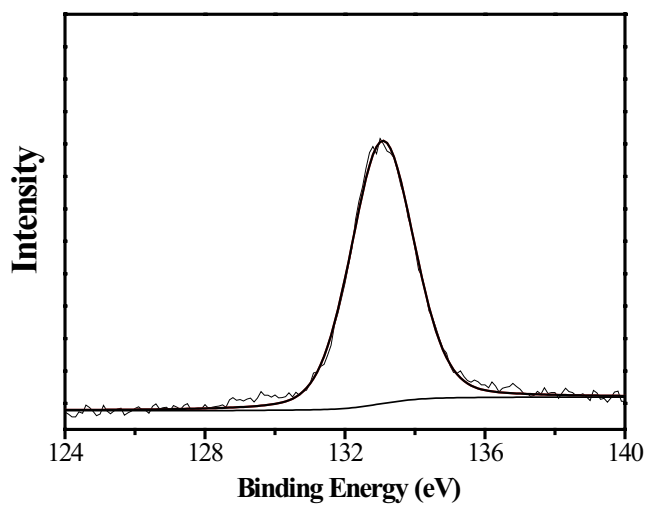


Fig. S4. High-resolution XPS spectrum of P 2p on the P-loaded adsorbent.